Catalysis Letters
https://doi.org/10.1007/s10562-023-04347-6

Sonocatalytic Degradation of Methylene Blue by a Novel SnO_2-Fe_3O_4@MWCNT Hybrid Nanocatalyst Under Ultrasonic Irradiation

Adem Yurtseven[1] · Bilge Ince[1] · Mehmet Salih Nas[2,3] · Mehmet Harbi Calimli[3,4]

Received: 12 February 2023 / Accepted: 16 April 2023

Abstract

In the present work, SnO_2-Fe_3O_4@MWCNT nanocatalyst was fabricated according to a sonochemical-hydrothermal procedure. The surface morphology and structure analyses of the synthesized SnO_2-Fe_3O_4@MWCNT were investigated by transmission electron microscope (TEM), X-ray diffraction (XRD), Raman spectroscopy, EDS, FTIR and BET analyses. The degradation efficiency of SnO_2-Fe_3O_4@MWCNT nanocatalyst in MB solution was tested by several experimental conditions such as SnO_2-Fe_3O_4@MWCNT dosage (8–20 mg/L), initial MB concentration (20–50 mg/L), initial solution pH (5–9), and ultrasonic output power (37–60 kHz). SnO_2-Fe_3O_4@MWCNT nanocatalyst retained its efficiency as 85% at common experimental conditions of 16 mg/L of SnO_2-Fe_3O_4@MWCNTs, 45 mg/L of MB, pH of 8, H_2O_2 of 15 mM, and 60 kHz in 60 min under ultrasonic irradiation. In addition, the optimum experiment conditions for SnO_2-Fe_3O_4@MWCNTs in MB degradation were investigated. The experiment result showed that the degradation efficiency of MB was increased by adding H_2O_2 to the reaction medium due to forming more free radicals. Further, it was detected that OH• radicals were determined to be the dominant oxidative species in MB degradation using SnO_2-Fe_3O_4@MWCNT catalyst. The reuse tests showed that SnO_2-Fe_3O_4@MWCNT sonocatalyst preserved its very stable structure after using the same catalyst 5 times. The intermediates and by-products after MB degradation using the catalyst were indicated by GC–MS analysis. Overall the results showed that the SnO_2-Fe_3O_4@MWCNT sonocatalyst has excellent potential for treating organic pollutants in wastewater.

✉ Mehmet Harbi Calimli
calimli.6500@gmail.com

[1] Civil Engineering, Faculty of Engineering, Hasan Kalyoncu University, Gaziantep, Turkey

[2] Department of Organic Agriculture Management, Faculty of Applied Sciences, Igdir University, 76000 Igdir, Turkey

[3] Research Laboratory Application and Research Center (ALUM), Iğdır University, 76000 Iğdır, Turkey

[4] Department of Medical Services and Techniques, Tuzluca Vocational School, Iğdır University, Iğdır, Turkey

Published online: 27 April 2023

Graphical Abstract

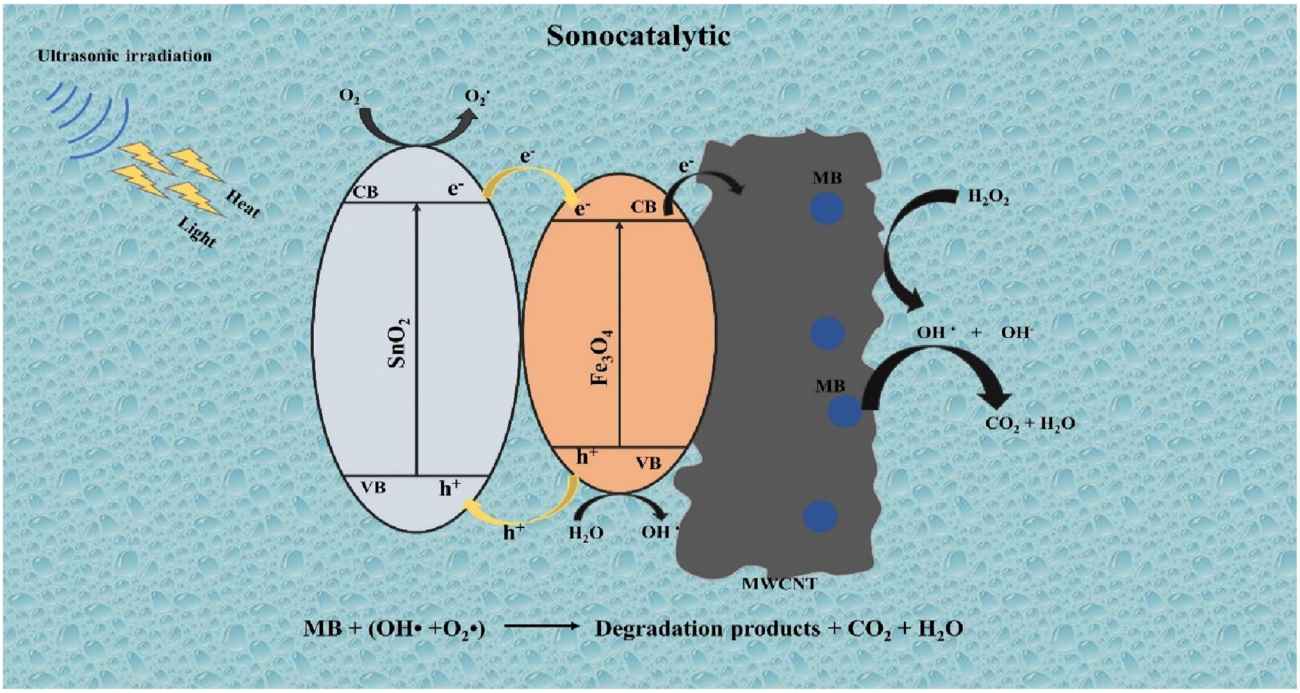

Keywords MB · Ultrasonic · Catalyst · Degradation · Efficiency

1 Introduction

Recently, dye pollutants originating from different industrial activities such as textile, cosmetics, paper, and paint constitute severe problems in the environment and natural life [1] The removal of polluting agents produced by industries is very important for the continuation of healthy living life. So far, many methods have been tried in the removal of paint and organic water contaminants. Among the methods, the sonocatalysis process has taken great importance due to some advantages like cost-effectiveness, sonolysis, complete elimination of organic pollutants, and a synergistic factor of sonocatalysis [2–4]. Thus, many studies have focused heavily on the sonocatalytic degradation of organic pollutants of different natures [5, 6]. In the sonocatalysis process, ultrasonic irradiation can lead to the generation of acoustic cavitation, causing the formation, release, and explosive collapse of bubbles in the aqueous reactant solution. Ahmadi et al. reported that the chemicals' synergic effect in the reaction during photo Fenton process could improve degradation efficiency [7]. Due to the collapse of the bubbles, OH• and O_2• radicals are formed by the thermal decomposition of water molecules, which causes the formation of temporary hot spot regions with high temperature and pressure. During the sonocatalytic process a light beam with broad wavelengths in the range from 200 to 800 nm (sonoluminescence) is simultaneously emitted [8–10]. Throughout the process, the sonoluminescence effect is created using different catalytic materials in the degradation of organic pollutants. Producing both emitted light and holes in the valence band by using a catalytic material, the electrons in the valence band of semiconductor materials can excite the conduction band [11]. In preparation of catalytical materials, semiconductor materials-based composite catalysts with different structures are intensely preferred to improve the sonocatalytic degradation efficiency of organic dyestuffs [12–17]. Tin (IV) oxide (SnO_2) is a semiconductor material that exhibits different properties like high optical, and excellent electrical. Because of these advantages, SnO_2 has been used in some research for the catalytic degradation of many organic dyes and compounds [18]. However, some properties of SnO_2 such as wide bandgap (3.6 eV) and high electron–hole pair recombination rate limit its effectiveness as a photocatalyst or sonocatalyst [19]. Recent studies have shown that integrating a multi-walled carbon nanotube (MWCNT) with SnO_2 results in a significant reduction in the energy bandgap [20], which is extremely important for its use in sonocatalytic activity. Because MWCNT is a conductivity-enhancing material

that reduces electron recombination resistance. In addition, in many studies, MWCNTs have been selected in the preparation of catalytical materials due to their other advantages such as high surface area and good electron conductivity [21]. Hence, adding MWCNT to the composition of the synthesized materials will be a good option to increase the catalytic properties in MB degradation [22]. Because of the advantages of MWCNT mentioned above, in this study, MWCNTs were preferred as the supporting material in catalyst synthesis for the degradation studies. Also, in the catalyst synthesis, Fe_3O_4 metal oxide was used as an active phase that caused the degradation of organic pollutants to increase in the sonocatalytical process. Doping of Fe_3O_4 in the material structure causes magnetization in the structure. There are successful studies in the literature on the doping of Fe_3O_4 to the material structure and the acquisition of magnetic properties [23, 24]. The incorporation of magnetic Fe_3O_4 nanoparticles (in the presence of an external magnetic field) provides the advantage of easy and fast phase separation in the sonocatalytic reactant environment. Further, the presence of Fe_3O_4 nanoparticles in the composition of the catalyst provides a synergistic effect that causes the sonocatalytic degradation to improve because of the formed additional binding sites and a more stable structure [25]. In this study, for the first time, SnO_2-Fe_3O_4@MWCNT nanocatalyst was prepared and its chemical and morphological properties were clarified with advanced analytical techniques. The prepared SnO_2-Fe_3O_4@MWCNT was effectively used in the sonocatalytic degradation of MB and the resulting reaction processes were elucidated.

2 Material and Methods

2.1 Materials

Multiwalled carbon nanotube (MWCNT), ferric chloride hexahydrate ($FeCl_3.6H_2O$, > 99.0%), $KMnO_4$, DMS, ferric chloride tetrahydrate ($FeCl_3.4H_2O$, > 99.0%) and tin chloride tetrahydrate ($SnCl_2$ $4H_2O$) materials were supplied from Sigma Aldrich. The chemicals of ethanol, methanol, butanol, and methylene blue were supplied by MERK. All of these chemicals we used in our studies were in analytical purity and used without any pretreatment. After washing all glass and metal experiment instruments were rinsed with distilled water and acetone and dried in an oven at 105 °C.

2.2 Instruments of Characterization

SnO_2-Fe_3O_4@MWCNT materials were investigated using TEM, XRD, Raman, FTIR, BET, EDS and GC–MS analysis devices to reveal their chemical and morphological structure. In TEM analyses of SnO_2-Fe_3O_4@MWCNT, a Hitachi HT7800 brand device with high resolution and contrast, which can reach 120 kV voltage, was used. A PANalytical EMPYREAN device, which can operate in a vacuum and inert gas environment that can reach 1200 °C, was used in XRD analyses. Raman analyses were performed with the Renishaw inVia Raman Microscope operating in a range of 532–735 nm. GC–MS analyses were conducted using Agilent 7820A GC with a Restek Column (100 m × 0.25 mm ID × 0.20 µm). The ultrasonic experiments were performed with a Bandaline brand device with an adjustable ultrasonic wave, experimental temperature, and power. Centrifugation studies were performed with a Hettich Universal 320 device. UV–Vis measurements were taken by Agilent Cary 60 instrument. FTIR analyses were taken with Agilent Cary 60. MICROMERITICS Tristar II brand devise was used to perform EDS analyses and Zeiss SmartEDX was used to carried out EDS analyses.

2.3 Preparation of SnO_2-Fe_3O_4@MWCNT Nanoparticles

2.3.1 Preparation of Fe_3O_4@MWCNT

The distribution of Fe_3O_4 metal oxide particles on the MWCNT surface was done using various physicochemical processes and an alkaline solution. In summary, firstly, a solution containing 1.18 g $FeCl_4$ $0.4H_2O$ and 2.35 g $FeCl_3.6H_2O$ in 150 mL water was prepared. An MWCNT mixture was prepared in another beaker (20 mL DMS) and sonicated for 15 min. These two mixtures were mixed in a beaker and the resulting mixture was kept under a nitrogen atmosphere at 80 °C for 30 min. After this time, 25% NH_4OH was added to the mixture to ensure the pH reached 9. The final mixture was mixed in a mechanical stirrer for 40 min at room conditions. The obtained Fe_3O_4@MWCNT was removed from the beaker using an external magnet and washed with abundant distilled water. The solid sample obtained was dried at 60 °C for 12 h [26].

2.3.2 Preparation of SnO_2-Fe_3O_4@MWCNT

A certain amount of Fe_3O_4@MWCNT and 0.77 g of $SnCl_2.4H_2O$ were taken and mixed in 50 mL water and sonicated for 10 min. 20 mL of 0.13 M $KMnO_2$ was added dropwise to the mixture. Over time, the color of the mixture turned into a dark brown color. The resulting mixture was then kept at 80 °C for 30 min. The resulting suspension was filtered, washed with abundant water, and kept at 60 °C for 12 h [27].

2.4 Degradation Experiments

The sonocatalytic effect of SnO_2-Fe_3O_4@MWCNT nanocatalyst on MB degradation was investigated by several steps as given below. The experimental setup was set up in an ultrasonic bath environment by fixing a 250 ml three-necked glass flask with gripper material. Before the beginning of the MB degradation experiment, a preliminary study was carried out to determine the adsorption–desorption equilibrium time between the nanocatalyst and MB. The adsorption–desorption equilibrium time was detected to be approximately 30 min under a dark environment and with a stirred mixture. Thereafter MB dye degradation experiments were carried out under standard experimental parameters. For this, initially, 5 mL of the previously prepared stock solution was taken and transferred to a centrifuge tube at 8000 rpm for 10 min. The resulting solution was used to take absorbance measurements in a 664 nm wave spectrum by a UV–Vis device. The obtained values from UV measurements were used to determine the effectiveness of the nanocatalyst on dye degradation using the equations given below [28]

$$q_t = \frac{(\mathrm{Co} - \mathrm{Ct}).\mathrm{V}}{\mathrm{m}} \tag{1}$$

$$\%\mathrm{A} = \frac{(\mathrm{Co} - \mathrm{Ce}).100}{\mathrm{Co}} \tag{2}$$

In these equations, the dye concentration of the initial time is expressed with C_o, and the dye concentration of any time is expressed with C_t ($mg.L^{-1}$), respectively. m represents the total solution mass. The symbol C_e represents the amount of adsorption concentration at equilibrium. The symbol V (L) refers to the solution volume used and the amount of MB adsorbed and A represents the percentage of MB degraded.

3 Results and Discussion

3.1 Structural Analysis Studies of SnO_2-Fe_3O_4@MWCNT Catalyst

Transmission electron microscopy (TEM), X-ray diffraction (XRD), and Raman analysis devices were used to test the morphological surface properties of SnO_2-Fe_3O_4 distributions on multi-walled carbon nanotubes. The TEM analysis of the SnO_2-Fe_3O_4@MWCNT nanocatalyst was performed to observe the distribution of metal particles on the MWCNT support material as well as to test the average particle size [29]. TEM analyses were used to calculate the content information, morphological structure and particle

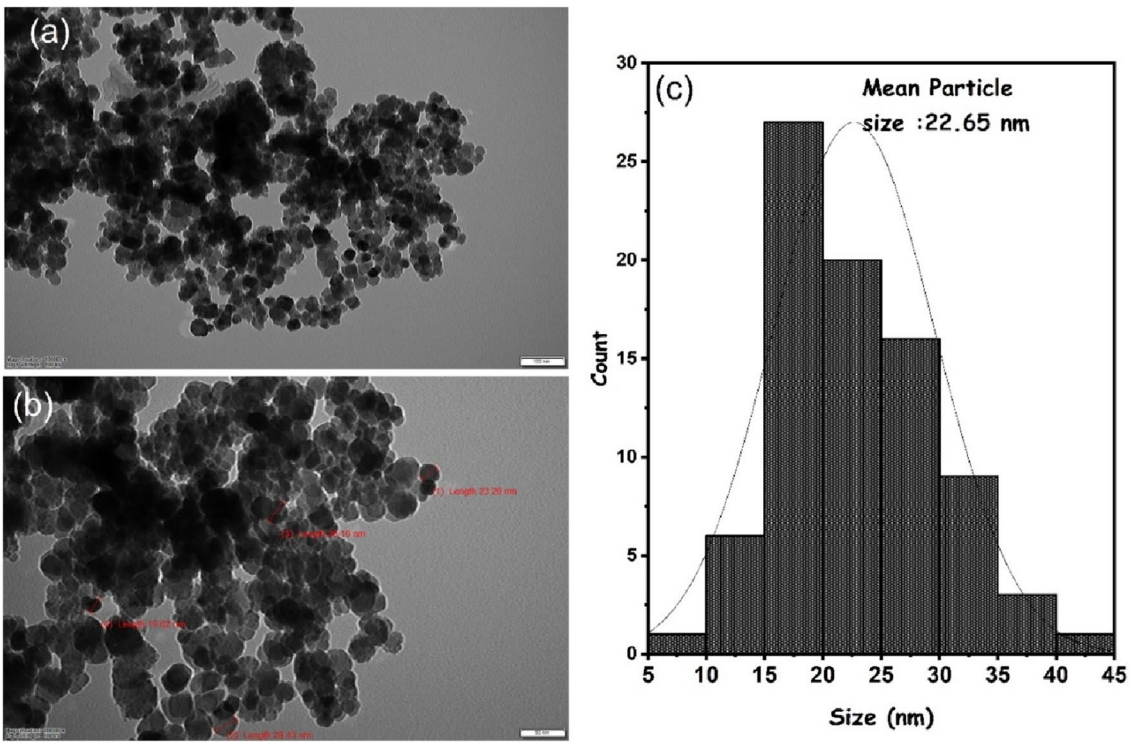

Fig.1 TEM analysis results with scales of 100 nm (**a**), 50 nm (**b**), and particle histogram (**c**)

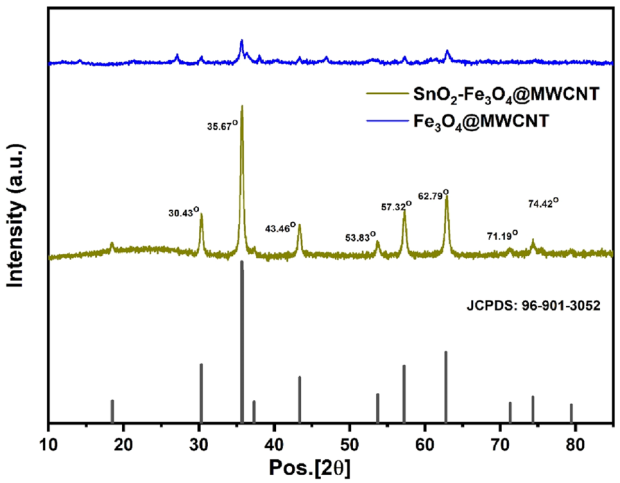

Fig. 2 XRD analysis results of the SnO_2-Fe_3O_4@MWCNT catalyst material materials

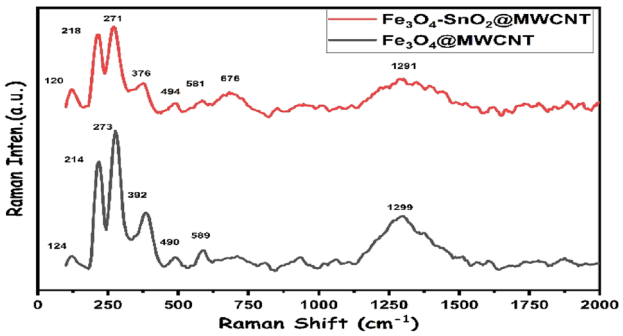

Fig. 3 Raman analyses of SnO_2-Fe_3O_4@MWCNT and Fe_3O_4@MWCNT catalyst materials

size of the material. In the TEM analysis of the prepared sample (Fig. 1), it is seen that SnO_2-Fe_3O_4 dispersed on the MWCNT surface and formed sphere-like nanostructures. The average particle size of SnO_2-Fe_3O_4@MWCNT nanocatalyst material was calculated by TEM analysis and a particle histogram plot showing the average particle size. As seen in TEM analysis, the structure formed was mostly composed of spherical particles and the mean particle size of the as-synthesized catalyst was calculated to be 22.65 nm on average.

XRD analyses of SnO_2-Fe_3O_4@MWCNT and Fe_3O_4@MWCNT nanocatalysts were conducted to detect the crystalline structure and specific XRD peaks of SnO_2-Fe_3O_4@MWCNT. The XRD analyses of the materials are given in Fig. 2. The peak values obtained for the catalyst materials are tried to be defined by comparing them with similar materials found in the previous literature. The determined diffraction planes of (511), (440), (220) and (400) correspond to the Fe_3O_4 compound [29]. The peaks of 26.83°, 30.43° in XRD analyses of Fe_3O_4@MWCNT show the presence of MWCNT. The peak values of $2\theta = 30.43°$, 35.67°, 43.46°, 53.83°, 57.32°, 62.79°, and 74.42° were determined to be very close to the values found for the SnO_2-Fe_3O_4 catalyst material in the literature. These results show that the peak values were found slightly different from the values in the literature, which can be attributed to the added components [30].

Raman analyses are widely used to examine the changes in carbon materials after functionalization [31]. To detect the variations in MWCNT, Raman analyses of Fe_3O_4@MWCNT and SnO_2-Fe_3O_4@MWCNT nanoparticles were performed as seen in Fig. 3. Raman analysis was implemented by scanning in the wavelength range of 200–1900 cm^{-1}. The 1291 and 1299 bands are indicative of the formation of bonds from non-covalent ferrous metals. The differences in peaks (581, 676 cm^3) seen in Raman analyses can be attributed to SnO_2 and the cationic interactions between MWCNT and SnO_2-Fe_3O_4.

EDS analysis results of SnO_2-Fe_3O_4@MWCNT were performed to detect the elemental amount as seen in Fig. 4. EDS analyses confirm the presence of C, O, Fe, and Sn elements with ratios of 2.20%, 41.03%, 26.89%, and 29.87%, respectively.

FTIR analyses of SnO_2-Fe_3O_4@MWCNT and Fe_3O_4@MWCNT were conducted to see the chemical composition and functional groups present in the synthesized materials as seen in Fig. 5. Various vibration peaks at 3405, 2958, 2086, 1998, 1700, 1631, 1352, 1078 and 1063, 995 cm^{-1} have appeared. The functional groups of C = C, C–H, and C–C present in MWNCT were found at 2086, 1631, and 1186 cm^{-1}. Peaks at a range of 580–638 cm^{-1} show vibrations of Fe–O bonds in Fe_3O_4. Peaks of 2986, 1703, 1199, and 1063 cm^{-1} seen in the FTIR of Fe_3O_4@MWCNT show the presence of C–H, C = O, C–O–C, and C–OH chemical bonds [32]. After adding SnO_2 to Fe_3O_4@MWCNT, a little bit few shifts have occurred in these vibrations as seen in the FTIR analyses results of SnO_2-Fe_3O_4@MWCNT. These chemical bonds show some chemical reactions between C and O elements has been taken place. Peaks of 1525, 1199, and 1078 cm^{-1} are very close to vibrations of O–Si–O [33].

BET analyzes were performed to determine the surface area and porosity of the synthesized SnO_2-Fe_3O_4@MWCNT material. The BET analyzes are shown in Fig. 6. BET surface area of SnO_2-Fe_3O_4@MWCNT material was determined as 62.3628 m^2/g. The pore volume of the material was found to be 0.188833 cm^3/g. Compared to the MWCNT-based oxide materials (MnO_2) in the literature, it is observed that the SnO_2-Fe_3O_4@MWCNT surface area increases have been increased. This feature is a situation found in oxide compounds with mesoporous structure [34].

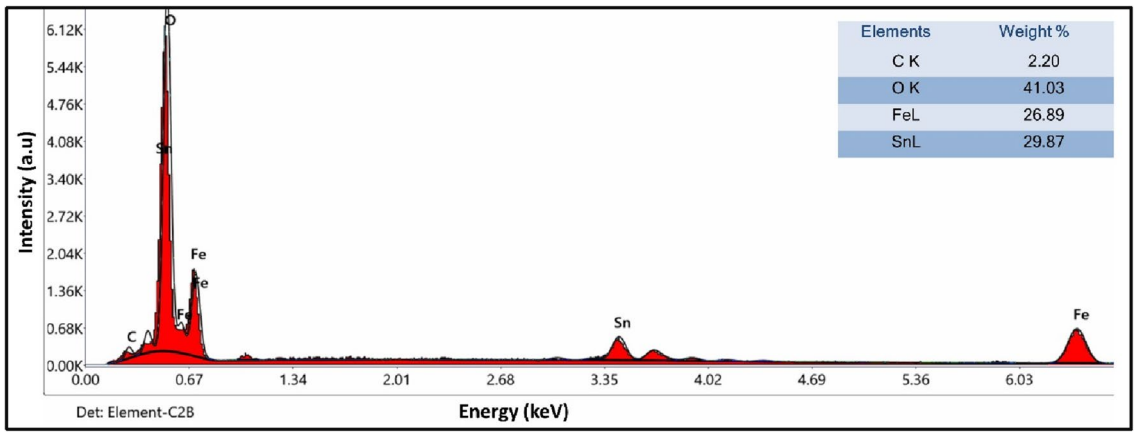

Fig. 4 EDS analyses of SnO_2-Fe_3O_4@MWCNT

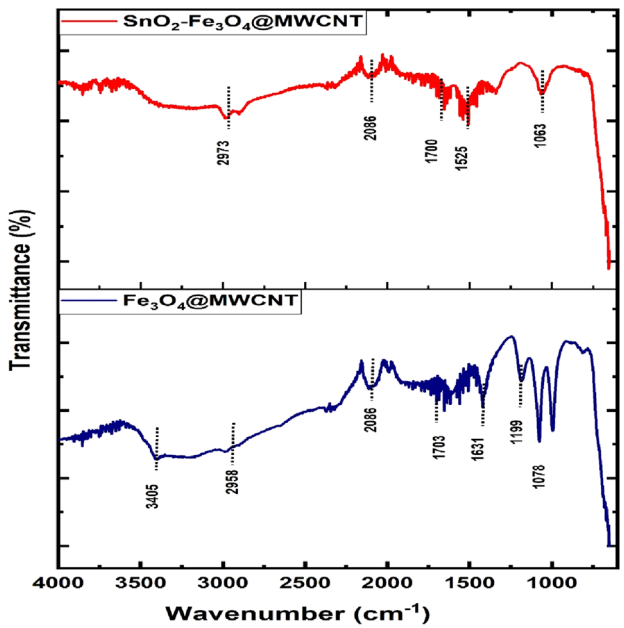

Fig. 5 FTIR analyses of SnO_2-Fe_3O_4@MWCNT and Fe_3O_4@MWCNT

3.2 Pre-Adsorption/Desorption Equilibrium Tests

The pre-adsorption/desorption equilibrium time of interval between the SnO_2-Fe_3O_4@MWCNT nanocatalyst and MB was performed in the absence of H_2O_2 and ultrasonic power parameters in a dark environment. The experimental results of pre-adsorption/desorption are given in Fig. 7a. The experiments at different pre-adsorption/desorption were carried out under common experiment conditions without H_2O_2. The adsorption/desorption experiments were conducted in 10–45 min. Also, the adsorption/desorption efficiency between SnO_2-Fe_3O_4@MWCNT and MB at different time intervals of 10, 15, 20, 25, 30, and 45 min was detected as 50.3%, 56.8%, 59%, 65.2%, and 69%, respectively. The data obtained from the pre-adsorption/desorption studies revealed that the adsorption/desorption equilibrium time intervals between SnO_2-Fe_3O_4@MWCNT catalyst and MB were observed to be 10–30 min. In light of these data, it can be said that 30 min is a sufficient time to reach the adsorption–desorption equilibrium for the current experiments.

3.3 MB Degradation Experiments at Different Ultrasonic Power and Temperature

In order to detect SnO_2-Fe_3O_4@MWCNT nanocatalyst effects at different ultrasonic powers and temperatures, various experiments were conducted and their results were given in Fig. 7b. As seen in Fig. 7b, SnO_2-Fe_3O_4@MWCNT nanocatalyst effects at different ultrasonic powers for the sonocatalytic MB degradation were studied at four different frequency ranges of 37–60 kHz in 60 min. The analysis data showed that the highest ultrasonic frequency for SnO_2-Fe_3O_4@MWCNT nanocatalyst in MB degradation was found to be 60 kHz. These findings can be explained in two different ways. First, high ultrasonic power led to a form of diffusion and this diffusion causes an increase in mass transfer, as a result, an increase in the MB degradation efficiency occurred. Secondly, the degradation of MB occurring in high frequencies causes high pressures—temperatures which result in the form of a sufficient electron–hole pair [35]. The results of SnO_2-Fe_3O_4@MWCNT nanocatalyst effects on MB degradation at different temperatures in a range of 298–328 K are given in Fig. 7c. The highest MB degradation efficiency (80%) using SnO_2-Fe_3O_4@MWCNT nanocatalyst was obtained at 318 K. This result can be attributed to the increased temperature causing an increase of activities of radicals (Kinetic energies of molecules) and the number of bubbles in the reaction medium [36]. The increased temperature accelerates the interactions of the excess bubble on

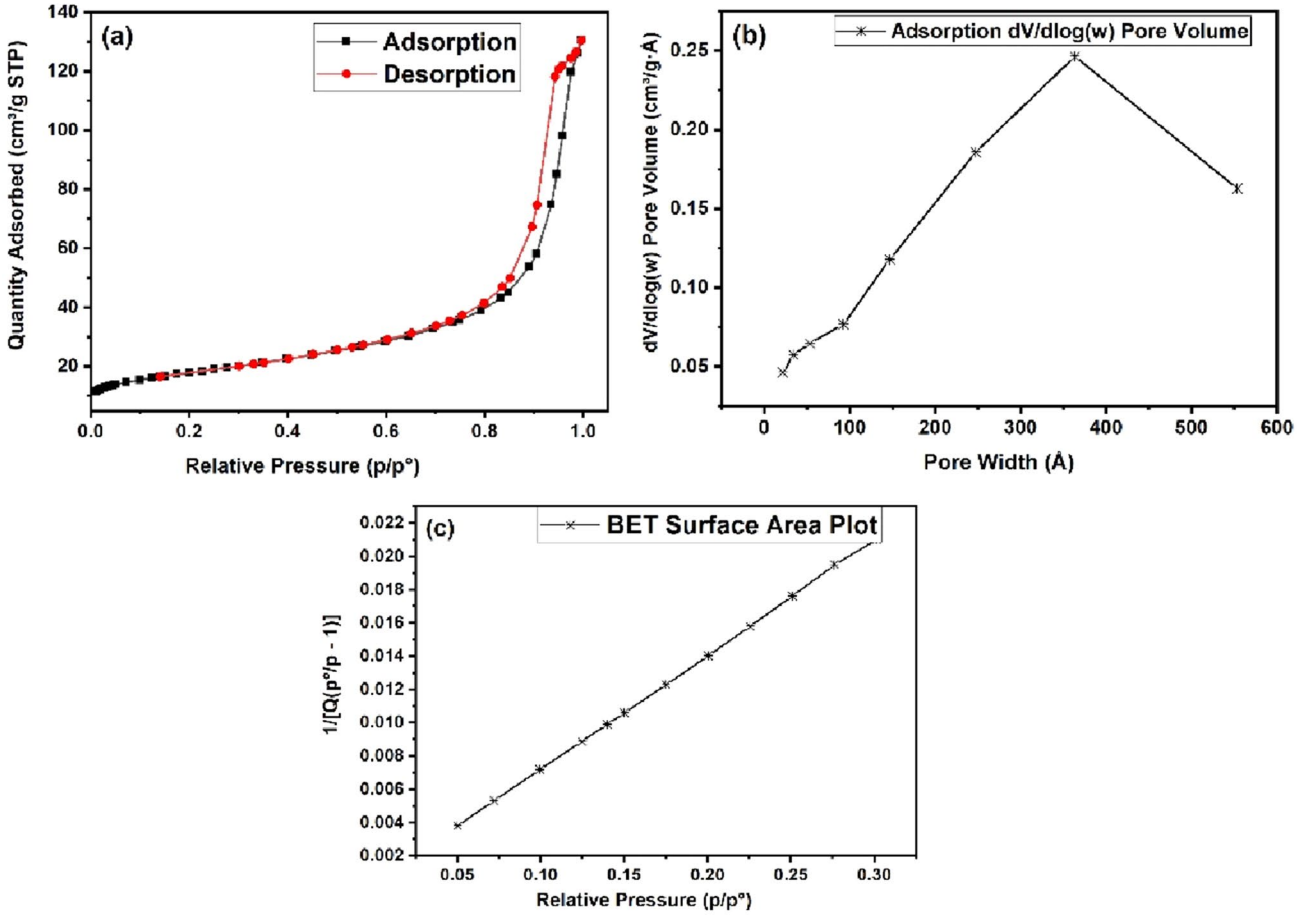

Fig. 6 Adsorption/desorption (**a**), volume distribution (**b**) and BET surface area (**c**) analysis results of SnO_2-Fe_3O_4@MWCNT

the catalyst surface and the dye, which causes to increase in the number of active radicals that are effective in the degradation process. As the dye structure deteriorated above 318 K the degradation efficiency of MB with SnO_2-Fe_3O_4@MWCNT nanocatalyst has been decreased [37].

3.4 Effects of SnO_2-Fe_3O_4@MWCNT Catalyst Amount, and MB Concentration on the Degradation Efficiency

The amount of catalyst is one of the most important parameter functions in MB degradation efficiency under specified conditions [38]. Four different experiments were conducted to detect SnO_2-Fe_3O_4@MWCNT catalyst effects on MB degradation and their results are given in Fig. 8a. As seen, as the amount of catalyst increased in the ultrasonic reaction medium, MB degradation efficiency increased. The most suitable catalyst dose value for maximum MB degradation efficiency was determined to be 16 mg L^{-1}. As can be expected that the increased SnO_2-Fe_3O_4@MWCNT catalyst amount increased the number of active sides present on the catalyst surface which is very effective in the degradation process. The degradation efficiency of MB using SnO_2-Fe_3O_4@MWCNT catalyst was observed to be decreased at above 16 mg L^{-1} catalyst concentration. This can be attributed that the active sides of the catalyst being covered with byproducts from MB degradation. In this case, fewer $OH^{\bullet}$ radical molecules are produced and released into the environment. As expected, over 16 mg. L^{-1}, decreasing active site and active radical number caused a decrease in MB degradation efficiency. Further, using more than 16 mg of SnO_2-Fe_3O_4@MWCNT catalyst amount in the reaction solution may result in the prevention of ultrasonic wave penetration into the reaction medium. However, SnO_2-Fe_3O_4@MWCNT nanoparticles tend to aggregate when used under high-concentration conditions, and this can be attributed to restricting the active molecules making them less present in the reaction medium (Fig. 8a). In addition, nanocatalyst used in large quantities supports the adsorption event. However, the excessive use of catalysts in the process environment causes fewer ultrasound waves and cavitations to the areas close to the catalyst surface [39, 40]. In order to see the

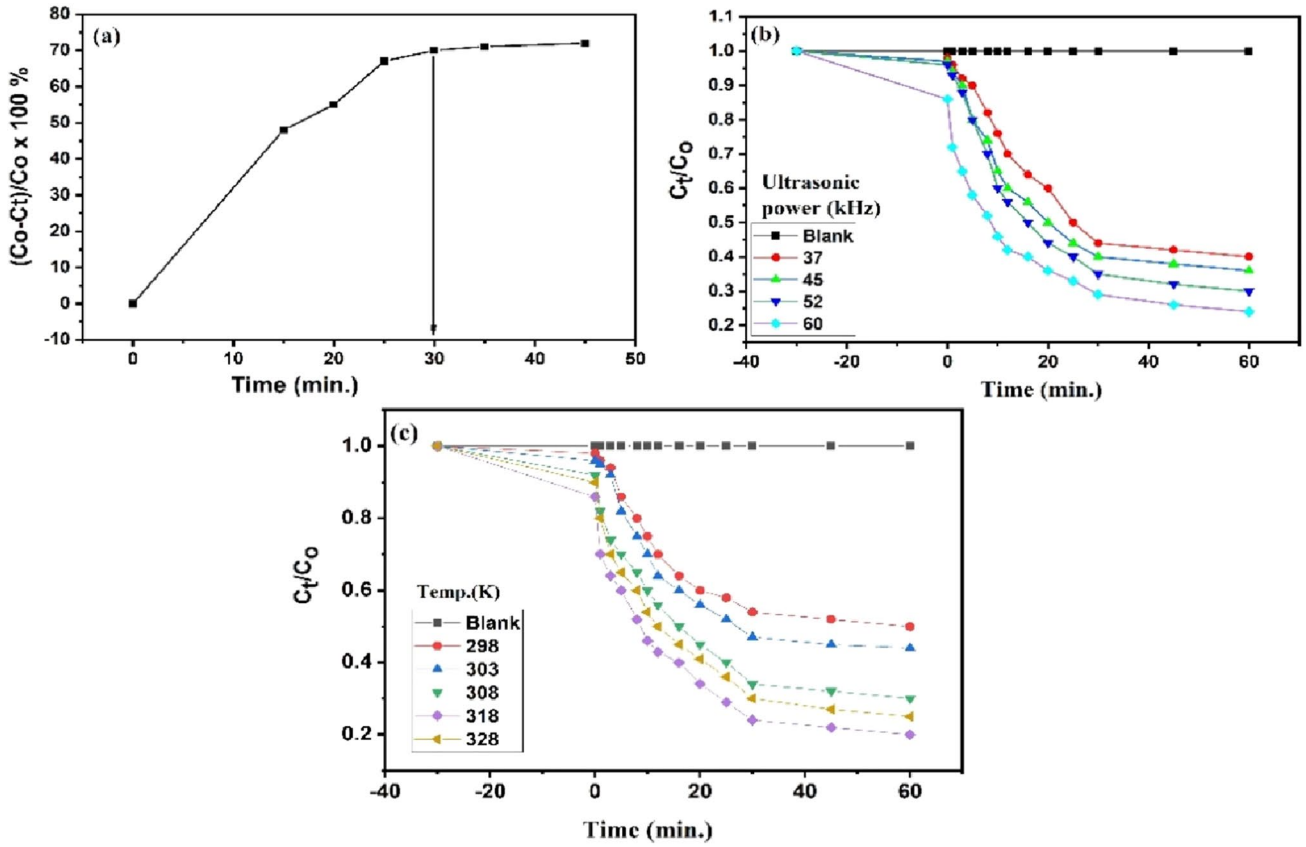

Fig. 7 Pre- Adsorption/desorption equilibrium experiment results (**a**), Ultrasonic Power experiments and (**b**) Experiments at different temperatures. Common parmeters: [MB] = 33 mg.L^{-1}, [H_2O_2] = 10 mM, [T] = 303 K, [Catal.] = 12 mg.L.$^{-1}$ and pH = 7)

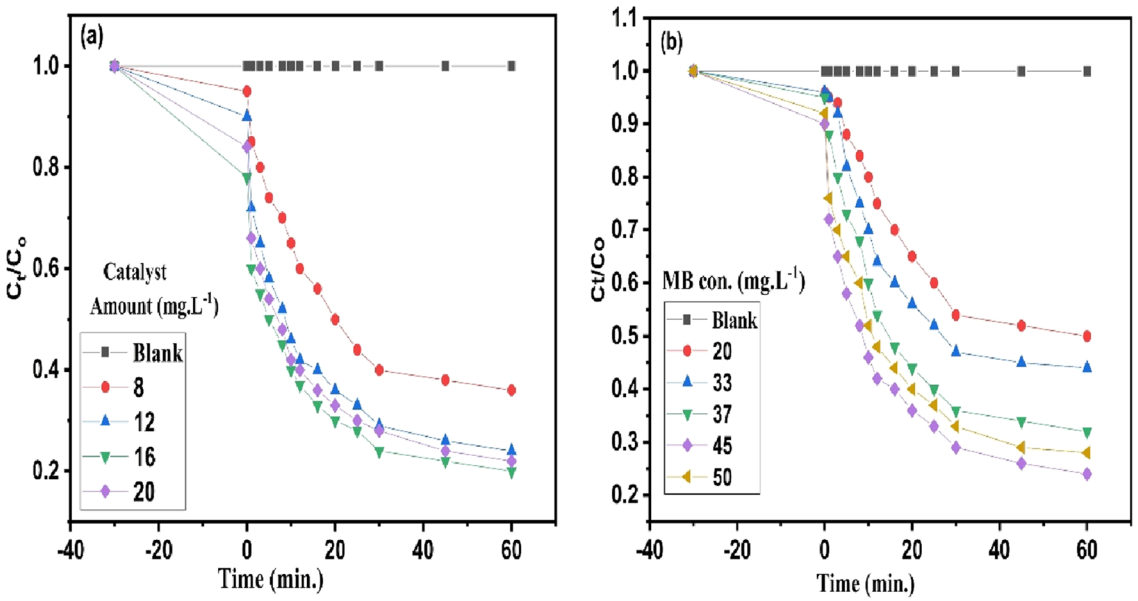

Fig. 8 MB degradation experiments with different catalyst amounts (**a**) and MB Concentrations (**b**) (Common Parameters: T = 303 K, Frequency = 60 kHz, [H_2O_2] = 10 mM, and pH = 7)

Table 1 Experimental findings of some catalysts used in MB degradation

Catalysts	Dyes	Time (min)	Irradiation type	Degradation (%)	References
AgCu@MWCNT	MB	60	Us	90.2	[52]
CdSe/GQDs	MB	90	Us	99	[53]
MGZ@SiO_2	MB	60	Us	95	[54]
SnO_2/MWCNT	MB	30	Us	98	[55]
$AgFe_2O_4$@MWCNT	MB	75	Us	98.5	[3]
TiO_2-CNT	MB	120	Us	100	[56]
ZnO/GR/TiO_2	MB	120	Us	79	[57]
ZnO–bs	MB	90	Us	77.8	[58]
AgBr	MB	180	Us	48	[59]
Fe_3O_4/Mn_3O_4/CuO	MB	150	Us	95.04	[60]
SnO_2-Fe_3O_4@MWCNT Fe_3O_4@MWCNT Fe_3O_4@MWCNT	MB	60	Us	85	This work

effectiveness of SnO_2-Fe_3O_4@MWCNT catalyst particles on MB degradation efficiency from a broader perspective, some catalysts and their experimental results in literature studies were compared in Table 1. In ultrasonic-degradation processes, the effect of dye concentration is another important function parameter in the evaluation of MB dye degradation to detect the effectiveness of the catalyst used. The degradation of MB experiments in different MB concentrations in a range of 20–50 mg.L^{-1} was performed and their results are given in Fig. 8b. Sonocatalytic degradation efficiency of MB in different MB concentrations was performed under common conditions of 12 mg.L^{-1} SnO_2-Fe_3O_4@MWCNT dose, 10 mM H_2O_2 concentration, pH 7 solution, and 60 kHz ultrasonic frequency. The studies conducted at different MB concentrations showed that the highest sonocatalytic degradation efficiency of MB using SnO_2-Fe_3O_4@MWCNT was achieved at 45 mg.L^{-1} MB dye concentration. The use of more than 45 mg.L^{-1} MB caused a slight decrease in MB degradation activity. This situation can be explained by two different reasons. Firstly, the presence of excess MB in the medium causes the energy generated by the cavitations formed in ultrasonic conditions to be absorbed and its interaction with the dye to decrease [41]. This can both limit the production of OH• radicals and lead to a significant reduction in the amount of degradation of the MB dye. Secondly, intermediate products are formed due to the interaction between MB dye molecules and OH• radical oxides. These intermediate products prevent active OH• radicals from the degradation of MB in the reaction medium [42].

3.5 Effects of pH Change on MB Degradation Efficiency

The organic matter degradation efficiency is affected by pH change. The detecting pH effects on the degradation of organic pollutants like MB have been studied by some researchers [43]. To detect the effects of pH variations on MB degradation using SnO_2-Fe_3O_4@MWCNT catalyst 5 experiments with pH in a range of 5–9 were performed. The experimental results using the SnO_2-Fe_3O_4@MWCNT catalyst are given in Fig. 9a. It was found that there was an increase in MB degradation efficiency with increasing pH. Maximum MB degradation efficiency was found at pH 8. As it is known, pH affects the amount of charge on the catalyst surface in the environment [44, 45]. In addition, pH affects the oxidizing species formed between the dye and the catalyst. In this way, it also provides a synergistic effect between the substance in the catalyst structure and the substrate. [46]. As can be seen from the test results, the interaction of the catalyst and MB dye is very low at pH 8 and below. As can be seen, a decrease in MB degradation was observed at pH 8 and below. Similar results can be seen in the previous studies [47]. However, as the pH value increased, an increased MB degradation was observed. This increased MB degradation can be explained by the synergistic effect on the nanocatalyst activity as a result of the increased negatively charged molecules in the reaction environment [48]. Studies conducted in a sonocatalytic process environment showed a significantly positive effect between the degradation concentration of MB and the pH function H/OH ion balance [49]. In addition, the pH state of the catalyst surface affects the dye degradation efficiency. Because, depending on the environment and catalyst surface pH, the attraction and interaction of the negative or positive active molecular changes. The amount of catalyst surface charge varies depending on the ambient pH. Additional to pH experiments, isoelectronic point experiments of the SnO_2-Fe_3O_4@MWCNT catalyst were performed. For this, nine solutions containing 20 mg catalyst in 50 mL of $NaNO_3$ with different pH (2–9) were prepared according to the literature [48]. The final pH values of the mixtures were measured at common conditions and room temperature. As shown in Fig. 9b–c, the pHzpc values of SnO_2-Fe_3O_4@

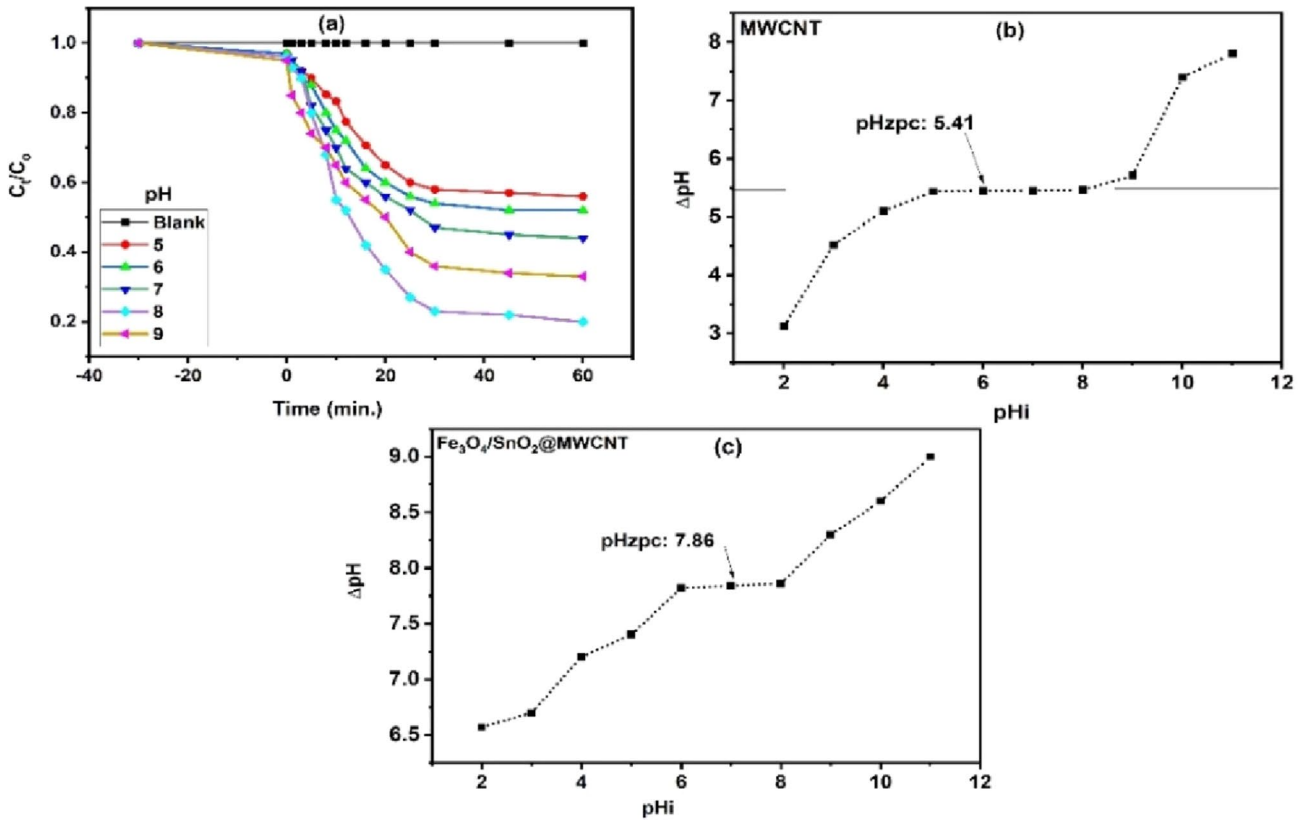

Fig. 9 **a** pH change experiment results, **b** zero point of MWCNT, **c** Zero-point of SnO_2-Fe_3O_4@MWCNT, (Common parameters; Frequency = 60 kHz, [T] = 303 K, [MB] = 33 mg.L^{-1}, [H_2O_2] = 10 mM, T = 303 K, and [Catal.] = 12 mg.$L.^{-1}$)

MWCNT nanocatalyst particle and MWCNT were obtained as 7.86 and 5.41, respectively. The net surface charge amount at this pH point of the SnO_2-Fe_3O_4@MWCNT nanocatalyst particle is zero. If the pH of the reaction medium is below 7.86, the surface charge of the nanocatalyst particle is positive, and over 7.86, the nanocatalyst surface charge will be negatively charged [50, 51]. Considering these data of pH experiments, the optimum pH value for MB degradation was determined to be 8. This result can be expressed as a result of the increase in the number of $OH^{\bullet}$, $O_2^{\bullet}$ oxidizing radical species (about 80%) which are extremely effective on MB degradation [39].

3.6 H_2O_2 Concentration

In the mechanism of the ultrasonic process, the amount of H_2O_2 concentration is the parameter that directly affects active radical formation on dye degradation [61, 62]. As displayed in Fig. 10a, the optimal concentration of H_2O_2 for MB degradation under common experiment conditions was detected to be 15 mM. At concentrations of H_2O_2 above 15 mM, a slight decrease in the catalytic dye degradation efficiency was observed. As investigated in Eqs. 3 and 4, in high concentrations of H_2O_2, H_2O_2 acts as a scavenging for OH• radicals which are required in oxidation reactions [63, 64]. On the other hand, under conditions of low H_2O_2 concentration, a small amount of OH• radicals are formed, and in this case, a decrease in the amount of degraded MB takes place. According to this information in the literature, it has been found that keeping the amount of H_2O_2 in the reaction medium at a certain rate affects the organic matter degradation rate. H_2O_2 triggers the OH• formation reaction as a result of its interaction with the catalyst surface. Here, H_2O_2 acts as an electron acceptor. As a result of the interaction of h^+ and OH^- ions, OH• radical formation occurs (Eq. 6). As seen in Eqs. 7 and 8, H_2O_2 turns into water and O_2 molecules. O_2• radicals are formed as a result of the interaction of O_2 with the electrons present in the reaction medium. As seen in Eqs. 9 and 10, it can be said that OH• radicals are more effective on MB degradation than O_2• radicals. Similar results have also been reported in some studies [65]. Considering all these possible reactions, it can be said that the use of H_2O_2 molecules in MB degradation under specified fixed conditions is extremely effective. Also, the effect on MB degradation via heterogeneous sono-Fenton-like processes was tested by adding some scavengers like t-BuOH, EtOH, and MeOH to investigate the scavenging working reactant process. Figure 10b shows

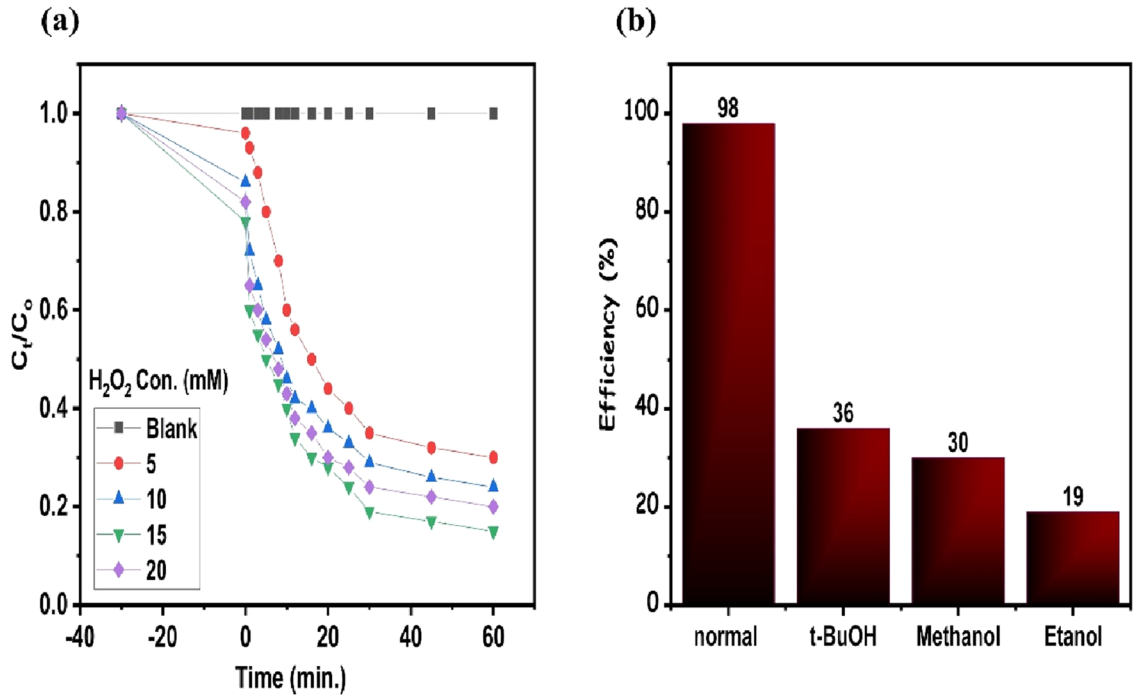

Fig. 10 H_2O_2 Concentration (**a**) and Scavengers efficiency (**b**) (Experimental conditions:[MB] = 33 mg.L^{-1}, [T] = 303 K, [cat.] = 12 mg.L^{-1}, and frequency = 60 kHz.)

the experiment results performed with different scavengers catalyzed SnO_2-Fe_3O_4@MWCNT nanparticle in MB degradation. The addition of 5 mL of t-BuOH, MeOH, and EtOH in reaction medium provided an effective reduction in MB removal efficiency from 85 to 36%, 30%, and 19%, respectively. To conclude that, we can say that these scavengers turned out to have a dramatic effect on MB degradation.

$$H_2O_2 + OH^{\bullet} \rightarrow H_2O + HOO^{\bullet} \quad (3)$$

$$HO_2 + OH^{\bullet} \rightarrow H_2O + O_2 \quad (4)$$

$$H_2O_2 + e^- \rightarrow H_2O + HO^{\bullet} + OH^- \quad (5)$$

$$h^+ + OH^- \rightarrow OH^{\bullet} \quad (6)$$

$$H_2O_2 \rightarrow H_2O + 1/2O_2^{\bullet} \quad (7)$$

$$O_2 + e^- \rightarrow O_2^{\bullet} \quad (8)$$

$$^{\bullet}OH + MB \rightarrow \text{products} \quad (9)$$

$$^{\bullet}O_2^- + MB \rightarrow \text{products} \quad (10)$$

3.7 Effects of the Reaction Medium on MB Degradation Efficiency

Figure 11a shows the test results of MB degradation performed at different experiment conditions with and without some parameters. The effects of these variable factors on MB degradation in the presence of the determined main parameter were tested using the UV device (Fig. 11b). As can be seen in Fig. 11a, there is little change in MB degradation efficiency in MB degradation experiments performed only in the presence of Us. In the presence of Us + H_2O_2, a slight increase in the post-catalytic effect on dye degradation was observed compared to the first variation (Only Us). Similarly, it can be seen from these results, it is seen that there is an increase in MB degradation efficiency with the addition of a catalyst to the reaction medium. By adding H_2O_2, it has been observed an increased catalytical MB degradation efficiency. Similar behaviors can be seen by incorporating other agents like a catalyst, Uv light, etc. in the reaction medium. In this case, it is easily seen that H_2O_2 is the source of active species such as OH• required for MB degradation. In the presence of Fe_3O_4@MWCNT the sonocatalytic performance on MB degradation was experimentally obtained as 40% at the constant parameters as seen in Fig. 11b. However, in the presence of Us/SnO_2-Fe_3O_4@MWCNT/H_2O_2 in the experimental environment, extremely remarkable results of the MB

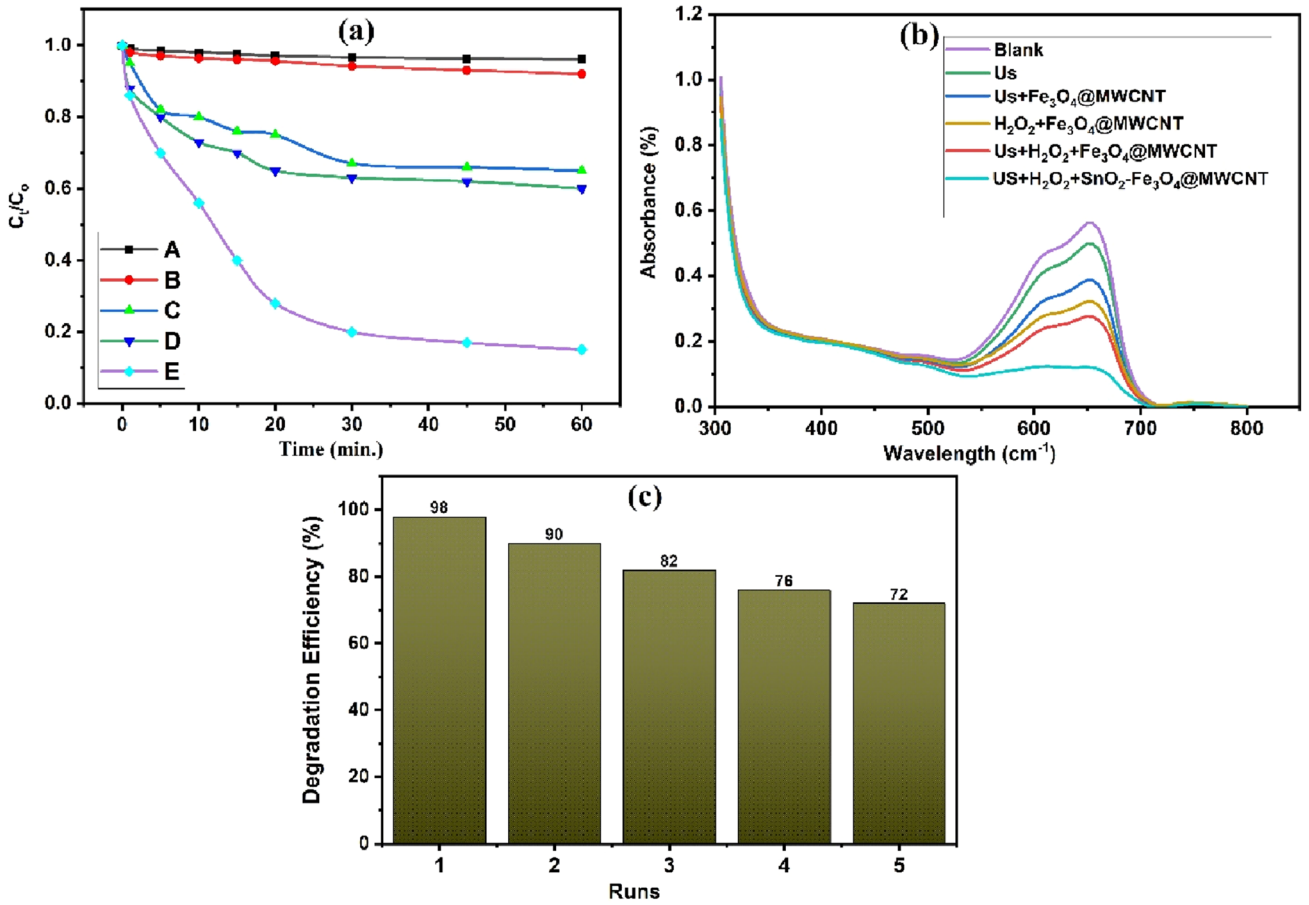

Fig. 11 **a** Different environmental conditions (A)Us, (B) Us + H_2O_2, (C) SnO_2-Fe_3O_4@MWCNT, (D) Us + SnO_2-Fe_3O_4@MWCNT, and (E) Us + H_2O_2 + SnO_2-Fe_3O_4@MWCNT, **b** MB absorbance experiments depending on different ambient conditions, and **c** Reuse experiment results (Common Parameters [MB] = 33 mg.L^{-1}, [T] = 303 K, [Catal.] = 12 mg, and Frequency = 60 kHz.)

degradation efficiency were obtained in the sonocatalytic process study (With a degradation efficiency of about 85% in 60 min). From these results, it can be said that ultrasonic irradiation enables sonoluminescence and the production of high amounts of visible light. Visible light has a relatively wide wavelength range due to acoustic gaps. When exposed to ultrasonic light, the MWCNT and SnO_2-Fe_3O_4 structures in the synthesized catalyst produce gaps and excited structures in the valence bands. These excited electrons move from the valence band to the conduction band. As a result, electrons in the conduction band of SnO_2 and Fe_3O_4 are transferred to the conduction band of MWCNT with ultrasonic light. As can be seen from Scheme 1, the sonogized gaps in the valence band (VB) of SnO_2-Fe_3O_4 allow the electrons in MWCNT to move easily. In this way, sonogicholes and electrons move bidirectionally, resulting in increased recombination rate and charge efficiency. Thus, a synergy of sonic matter and ultrasonic frequency is formed [66–68]. OH• radicals are formed as a result of the interaction of electrons in the conduction band (CB) with H_2O_2. The OH• radicals formed also take an active role in the decomposition of MB. Based on all the predicted results above, a sonogenization electron–hole separation mechanism using SnO_2-Fe_3O_4@MWCNT catalyst in the presence of sonocatalytic process was proposed and illustrated in Scheme 1.

As seen in Eq. (11), the interaction of SnO_2-Fe_3O_4@MWCNT nanocatalyst particle surface with H_2O_2 molecules had a great synergistic effect on the increase of OH• radicals. In this case, we can say that it makes a positive contribution in terms of MB degradation [69]. In our study, in the sonocatalytic process medium based on Us + SnO_2-Fe_3O_4@MWCNT + H_2O_2 medium, the catalyst in the solution medium was exposed to ultrasonic waves and dispersed homogeneously. In this way, it was ensured that the catalyst was dispersed in the entire reaction medium. Homogeneous distribution is required for the active sites of the catalyst to be fully ubiquitous. As can be seen in Eqs. 11 and 12, $OH^{\bullet}$ radical formation occurred with the sonocatalytic process [70]. Based on these data, we can state that a highly effective metallic nanocatalyst in MB degradation

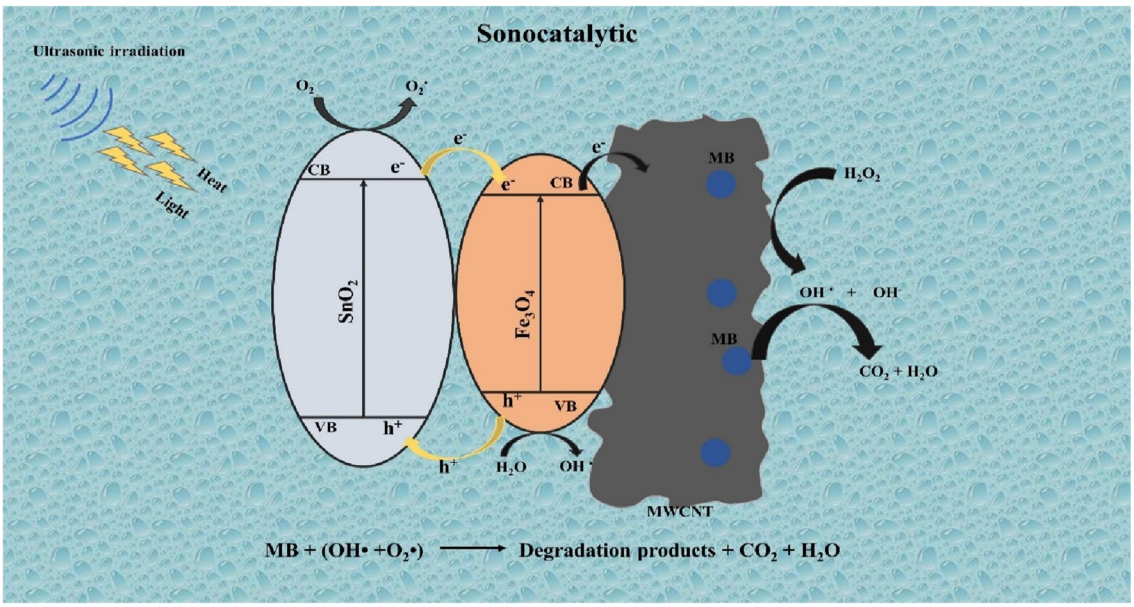

Scheme 1 Possible mechanism of sonocatalytic degradation in the interaction of Methylene Blue dye with SnO_2-Fe_3O_4@MWCNT nanocatalyst

under the Us + SnO_2-Fe_3O_4@MWCNT + H_2O_2 parameter has been produced.

$$SnO_2 - Fe_3O_4@MWCNT + Us \rightarrow SnO_2 - Fe_3O_4@MWCNT\,(h + e-) \quad (11)$$

$$SnO_2 - Fe_3O_4@MWCNT\,(e-) + H_2O_2 \rightarrow SnO_2 - Fe_3O_4@MWCNT\,(e-) + OH\bullet + OH- . \quad (12)$$

3.8 Reuse of SnO_2-Fe_3O_4@MWCNT Catalyst and MB Degradation Products

Reuse tests are widely performed to detect the effectiveness of catalytical materials [71]. Thus, in this study, the reuse of the SnO_2-Fe_3O_4@MWCNT catalyst was tested to evaluate its effectiveness in MB degradation conducted 5 runs (Fig. 11c). The reuse experiments of the SnO_2-Fe_3O_4@MWCNT catalyst we produced were carried out under common experimental parameters at 30 °C temperature, 33 mg.L^{-1} dye amount, 60 kHz ultrasonic wave frequency, 12 mg.L^{-1} catalyst amount, and at 75 min. Briefly, the reuse experiments were carried out as follows. At the end of the first experiment carried out under standard conditions, the catalyst in the environment was removed, washed, and dried. The second experiment was started again by introducing the catalyst back into the reaction medium. In this way, 5 reuse experiments were carried out and their results are given in Fig. 11c. As can be seen from the experimental results, it was determined that there was a 25.6% decrease in the usage efficiency of the SnO_2-Fe_3O_4@MWCNT catalyst after 5 experiments. It can be deduced that the stability of the MWCNT-formed structure, which is added to the catalyst structure, affects its reuse. A stable SnO_2-Fe_3O_4@MWCNT catalyst is effective in minimizing ion leakage that occurs during 5 reuses. F_3O_4 in the structure provides the formation of the magnetic feature in the structure. However, SnO_2 increases the conductivity in the structure. These findings are in line with the previous studies [72]. In light of all the data, it has been proven that the SnO_2-Fe_3O_4@MWCNT nanoparticle is quite effective in MB degradation under ultrasonic conditions. In addition, GC–MS analyses of the products after MB decomposition using SnO_2-Fe_3O_4@MWCNT catalyst in sonocatalytic medium were applied. The products formed as a result of GC–MS analyses are given in Fig. 12. Generally, substances of Azure A, Azure B, Azure C, benzenesulfonic acid, 1,3 dimethyl benzene, 1,6 hexane diamine, Methyl ester octadecanoic acid, hexadecanoic acid, Naphthalene, 1-ethyl butyl, and trichloromethane were identified from GC–MS analyses.

3.9 Kinetic Studies

In order to compare the sonocatalytic activity of the obtained nanoparticles, kinetic studies are applied under optimum conditions. For this, Eq. 13 Langmuir Hinshelwoo kinetic model given below is used.

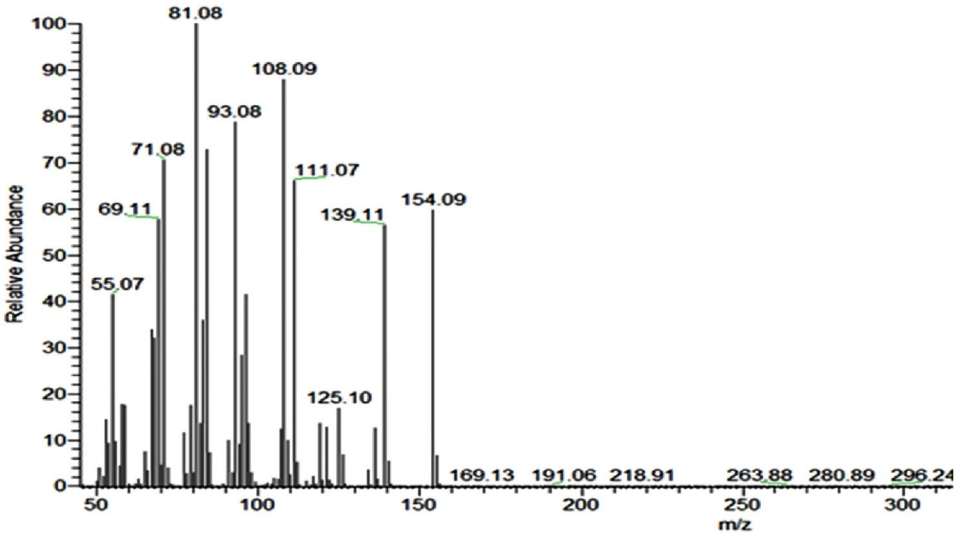

Fig. 12 By-products formed after MB degradation catalyzed with SnO_2-Fe_3O_4@MWCNT nanoparticles detected using GC–MS analyses

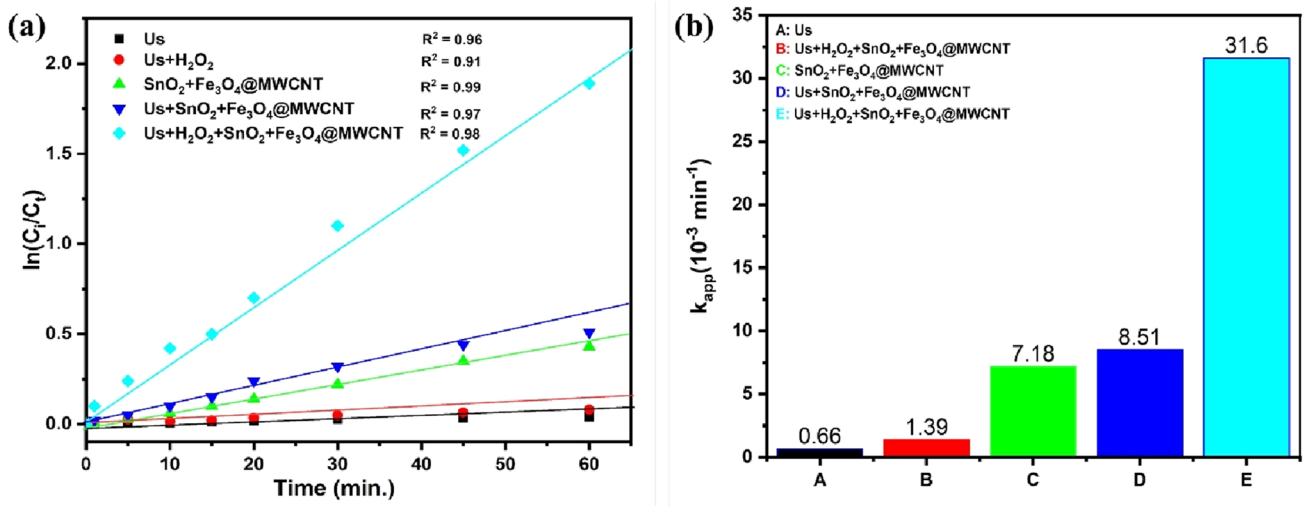

Fig. 13 **a** LH pseudo-first-order kinetic model for MB sonodegradation on each of the samples prepared under optimized conditions (catalyst loading: 16 $mg.L^{-1}$, pH: 8 and [MB]: 45 $mg.L^{-1}$), and **b** MB degradation under various kinetic conditions kinetic data

$$\ln\left(\frac{C_i}{C_r}\right) = k_{app}.t \tag{13}$$

In Eq. 13, C_r and C_r represent the primary and residual concentrations of MB dye at 0 and any t times, respectively. k_{app} represents the apparent velocity coefficient. As can be seen in Eq. 13, the apparent rate constant (k_{aap}) was calculated on the linear graph drawn between $\ln(C_i/C_r)$ and t and shown in Fig. 13a. Considering that the correlation coefficient (R^2) is greater than 0.90 in the presence of all reaction conditions, it was determined that the experimental results of MB sonodegradation by all the processes examined were positively consistent with the LH pseudo-first-order kinetic model, which is compatible the literature [73, 74]. Figure 13b shows the changes in kapp value in the presence of different reaction conditions. Based on this kinetic model, the calculated rate constants of Us alone, $Us + H_2O_2$, $SnO_2 + Fe_3O_4$@MWCNT, $Us + SnO_2 + Fe_3O_4$@MWCNT and $Us + H_2O_2 + SnO_2 + Fe_3O_4$@MWCNT in the presence of reaction conditions were found to be 0.66×10^{-3}, 1.39×10^{-3}, 7.18×10^{-3}, 8.51×10^{-3}, and 31.6×10^{-3} min^{-1}, respectively. These results showed that the rate of sonodecomposition of MB in $Us + H_2O_2 + SnO_2 + Fe_3O_4$@MWCNT was 47.87, 22.7, 4.40, and 3.71 times more efficient compared to Us alone, $Us + H_2O_2$, $SnO_2 + Fe_3O_4$@MWCNT,and $Us + SnO_2 + Fe_3O_4$@MWCNT, respectively. Also, the synergy factor was calculated as expressed in Eq. 14 and its synergistic effect was verified by testing. To further evaluate its efficacy in the presence of $Us + SnO_2 + Fe_3O_4$@MWCNT reaction conditions.

$$SynergyFactor = \frac{k_{\mathrm{Us+H2O2+SnO2+Fe3O4@MWCNT}}}{k_{\mathrm{Us}} + k_{Us+H2O2} + k_{\mathrm{SnO2+Fe3O4@MWCNT}} + k_{\mathrm{Us+SnO2+Fe3O4@MWCNT}}} \quad (14)$$

where $k_{Us+H_2O_2+SnO_2+Fe_3O_4@MWCNT}$, k_{Us}, $k_{Us+H_2O_2}$, $k_{SnO_2+Fe_3O_4@MWCNT}$ and $k_{Us+SnO_2+Fe_3O_4@MWCNT}$ are the apparent rate constants for $Us+H_2O_2+SnO_2+Fe_3O_4$@MWCNT, Us alone, $Us+H_2O_2$, $SnO_2+Fe_3O_4$@MWCNT,and $Us+SnO_2+Fe_3O_4$@MWCNT, respectively.

Synergy value data greater than 1 proves a highly effective integrated effect compared to individual effects, which is referred to as the synergistic effect. Further information related to synergistic effect can be seen in the literature [73, 75, 76]. Eq. (14), the synergy factor obtained in this study was found to be 1.78.

As can be clearly seen in Fig. 11a, complete decontamination of MB in the present study was achieved in a relatively shorter time in the presence of reaction conditions $Us+H_2O_2+SnO_2+Fe_3O_4$@MWCNT compared to the presence of other reaction conditions, which indicates the superior efficacy of MB in sonodegradation in the presence of reaction conditions $Us+H_2O_2+SnO_2+Fe_3O_4$@MWCNT. Therefore, in the presence of $Us+H_2O_2+SnO_2+Fe_3O_4$@MWCNT reaction conditions, SnO_2-Fe_3O_4@MWCNT nanoparticle is a highly effective catalyst that can be used for sonodecomposition of MB contaminations.

4 Conclusions

The findings of our study are briefly summarized below.

The SnO_2-Fe_3O_4@MWCNT catalyst was produced based on physicochemical and hydrothermal methods. Some advanced analytical methods such as XRD, TEM, Raman, EDS, FTIR and BET were used to elucidate the morphological and chemical properties of the formed catalyst.

The most suitable experimental conditions were determined for the SnO_2-Fe_3O_4@MWCNT catalyst, with a degradation efficiency of 85% MB dye. These conditions are 318 K temperature, 8 pH, 45 mg.L^{-1} dye concentration, 16 mg.L^{-1} catalyst amount and 60 kHz ultrasonic frequency.

It was found that the MB degradation rate increased with increased H_2O_2 concentration in the reaction medium. H_2O_2 caused an increase in the number of OH• radical particles formed. Also, it was found that substances such as methanol, ethanol, and butanol caused a decrease in the number of OH radicals formed.

It has been found that the Fe_3O_4@MWCNT catalyst can be reused 5 times with a 28% yield reduction after reuse experiments.

GC–MC analyses showed that mother byproducts of Azure A, Azure B, Azure C, benzenesulfonic acid, 1,3 dimethyl benzene, 1,6 hexane diamine, Methyl ester octadecanoic acid, hexadecanoic acid, Naphthalene, 1-ethyl butyl, and trichloromethane are formed after MB degradation using Fe_3O_4@MWCNT catalyst.

As a result, it was found that the produced SnO_2-Fe_3O_4@MWCNT catalyst could be used as an alternative nanocatalyst in MB degradation studies.

Acknowledgements We would like to thank the Research Laboratory Application and Research Center (ALUM) for the support and facilities provided Instrumentation Centre at Igdir University.

Declarations

Conflict of interest No potential conflict of interest was reported by the author(s).

References

1. Carmen Z, Daniela S (2012) Textile organic dyes–characteristics, polluting effects and separation/elimination procedures from industrial effluents–a critical overview. Org Pollut Ten Years After Stock Conv-Environ Anal Updat 3:55–60. https://doi.org/10.5772/32373
2. Shao X, Lu W, Zhang R, Pan F (2013) Enhanced photocatalytic activity of TiO2-C hybrid aerogels for methylene blue degradation. Sci Rep 31(3):1–9. https://doi.org/10.1038/srep03018
3. Nas MS (2021) AgFe2O4/MWCNT nanoparticles as novel catalyst combined adsorption-sonocatalytic for the degradation of methylene blue under ultrasonic irradiation. J Environ Chem Eng 9:105207. https://doi.org/10.1016/J.JECE.2021.105207
4. Zhu L, Da MZ, Park CY et al (2013) Characterization and relative sonocatalytic efficiencies of a new MWCNT and CdS modified TiO2 catalysts and their application in the sonocatalytic degradation of rhodamine B. Ultrason Sonochem 20:478–484. https://doi.org/10.1016/j.ultsonch.2012.08.005
5. Zhang S, Tian H, Zhang S et al (2013) Enhanced sonocatalytic activity, kinetic analysis, and sonocatalytic mechanism for silver phosphate by Br modifying with ionic liquids. J Am Ceram Soc 96:3536–3543. https://doi.org/10.1111/JACE.12531
6. Eren Z, Ince NH (2010) Sonolytic and sonocatalytic degradation of azo dyes by low and high frequency ultrasound. J Hazard Mater 177:1019–1024. https://doi.org/10.1016/J.JHAZMAT.2010.01.021
7. Ahmadi M, Kakavandi B, Jorfi S, Azizi M (2017) Oxidative degradation of aniline and benzotriazole over PAC@FeIIFe2IIIO4: a recyclable catalyst in a heterogeneous photo-Fenton-like system. J Photochem Photobiol A Chem 336:42–53. https://doi.org/10.1016/J.JPHOTOCHEM.2016.12.014

8. Riesz P, Berdahl D, Christman CL (1985) Free radical generation by ultrasound in aqueous and nonaqueous solutions. Environ Health Perspect 64:233. https://doi.org/10.1289/EHP.8564233
9. Hiller RA, Putterman SJ, Weninger KR (1998) Time-resolved spectra of sonoluminescence. Phys Rev Lett 80:1090–1093. https://doi.org/10.1103/PHYSREVLETT.80.1090
10. Didenko YT (2002) Suslick KS (2002) The energy efficiency of formation of photons, radicals and ions during single-bubble cavitation. Nat 4186896(418):394–397. https://doi.org/10.1038/nature00895
11. Wang J, Ma T, Zhang Z et al (2006) Investigation on the sonocatalytic degradation of methyl orange in the presence of nanometer anatase and rutile TiO2 powders and comparison of their sonocatalytic activities. Desalination 195:294–305. https://doi.org/10.1016/J.DESAL.2005.12.007
12. H Z, G Z, Q Z, (2014) MnO2/CeO2 for catalytic ultrasonic degradation of methyl orange. Ultrason Sonochem 21:991–996. https://doi.org/10.1016/J.ULTSONCH.2013.12.002
13. Zhai Y, Li Y, Wang J et al (2013) Effective sonocatalytic degradation of organic dyes by using Er3+:YAlO3/TiO2–SnO2 under ultrasonic irradiation. J Mol Catal A Chem Complete. https://doi.org/10.1016/J.MOLCATA.2012.10.006
14. Wang J, Wang J, Zhou S et al (2014) Improvement of sonocatalytic activity of TiO2 by using Yb, N and F-doped Er3+:Y3Al5O12 for degradation of organic dyes. Ultrason Sonochem 21:84–92. https://doi.org/10.1016/J.ULTSONCH.2013.05.003
15. Da MZ, Oh WC (2011) Sonocatalytic degradation and catalytic activities for MB solution of Fe treated fullerene/TiO2 composite with different ultrasonic intensity. Ultrason Sonochem 18:757–764. https://doi.org/10.1016/j.ultsonch.2010.10.008
16. Bokhale NB, Bomble SD, Dalbhanjan RR et al (2014) Sonocatalytic and sonophotocatalytic degradation of rhodamine 6G containing wastewaters. Ultrason Sonochem 21:1797–1804. https://doi.org/10.1016/J.ULTSONCH.2014.03.022
17. Ahmad M, Ahmed E, Hong ZL et al (2014) Photocatalytic, sonocatalytic and sonophotocatalytic degradation of Rhodamine B using ZnO/CNTs composites photocatalysts. Ultrason Sonochem 21:761–773. https://doi.org/10.1016/J.ULTSONCH.2013.08.014
18. Solís-Casados D, Vigueras-Santiago E, Hernández-López S, Camacho-López MA (2009) Characterization and photocatalytic performance of tin oxide. Ind Eng Chem Res 48:1249–1252. https://doi.org/10.1021/IE800604U
19. Linsebigler AL, Lu G Jr, JTY, (2002) Photocatalysis on TiO2 surfaces: principles, mechanisms, and selected results. Chem Rev 95:735–758. https://doi.org/10.1021/CR00035A013
20. Zaman S, Xin J, Butt FK (2014) Wet chemistry synthesis of SnO2/MWCNTs nanocomposites and their tuning energy bandgap properties. Mater Lett 119:111–114. https://doi.org/10.1016/J.MATLET.2013.12.064
21. Dabees S, Tirth V, Mohamed A, Kamel BM (2021) Wear performance and mechanical properties of MWCNT/HDPE nanocomposites for gearing applications. J Mater Res Technol 12:2476–2488. https://doi.org/10.1016/J.JMRT.2020.09.129
22. Qi H, Lee J, Wang L et al (2016) Photocatalytic performance of titanium dioxide nanoparticles doped with multi-metals. J Adv Oxid Technol 19:302–309. https://doi.org/10.1515/jaots-2016-0214
23. Yeganeh M, Fallah Jokandan S, Rahmatinia M et al (2020) Catalytic ozonation assisted by Fe3O4@SiO2@TiO2 in the degradation of aniline from aqueous solution: modelling and optimisation by response surface methodology. Int J Environ Anal Chem 102:7863–7880. https://doi.org/10.1080/03067319.2020.1839440
24. Bashiri F, Khezri SM, Kalantary RR, Kakavandi B (2020) Enhanced photocatalytic degradation of metronidazole by TiO2 decorated on magnetic reduced graphene oxide: characterization, optimization and reaction mechanism studies. J Mol Liq 314:113608. https://doi.org/10.1016/J.MOLLIQ.2020.113608
25. Khataee A, Sheydaei M, Hassani A et al (2015) Sonocatalytic removal of an organic dye using TiO2/montmorillonite nanocomposite. Ultrason Sonochem 22:404–411. https://doi.org/10.1016/j.ultsonch.2014.07.002
26. Tourchi Moghadam MT, Seifi M, Askari MB, Azizi S (2022) ZnO-MWCNT @ Fe3O4 as a novel catalyst for methanol and ethanol oxidation. J Phys Chem Solids. https://doi.org/10.1016/j.jpcs.2022.110688
27. Yu L, Lan X, Wei C et al (2018) MWCNT/NiO-Fe3O4 hybrid nanotubes for efficient electromagnetic wave absorption. J Alloys Compd 748:111–116. https://doi.org/10.1016/J.JALLCOM.2018.03.147
28. Barhon Z, Bozon-Verduraz F,, ois, Saffaj N, et al (2011) Photodegradation of indigo carmine in aqueous solution by zirconium phosphates. Desalin Water Treat 30:69–73. https://doi.org/10.5004/dwt.2011.1394
29. Di Mauro A, Fragalà ME, Privitera V, Impellizzeri G (2017) ZnO for application in photocatalysis: From thin films to nanostructures. Mater Sci Semicond Process 69:44–51
30. Qureshi D, Behera H, Anis A et al (2020) Effect of polyglycerol polyricinoleate on the polymorphic transitions and physicochemical properties of mango butter. Food Chem 323:126834. https://doi.org/10.1016/J.FOODCHEM.2020.126834
31. Gong K, Du F, Xia Z et al (2009) Nitrogen-doped carbon nanotube arrays with high electrocatalytic activity for oxygen reduction. Science 323:760–764. https://doi.org/10.1126/science.1168049
32. Omer AM, Elgarhy GS, El-Subruiti GM et al (2023) Construction of efficient Ni-FeLDH@MWCNT@Cellulose acetate floatable microbeads for Cr(VI) removal: Performance and mechanism. Carbohydr Polym 311:120771. https://doi.org/10.1016/J.CARBPOL.2023.120771
33. Van Tran T, Turrell S, Eddafi M et al (2010) Investigations of the effects of the growth of SnO2 nanoparticles on the structural properties of glass–ceramic planar waveguides using Raman and FTIR spectroscopies. J Mol Struct 976:314–319. https://doi.org/10.1016/J.MOLSTRUC.2010.04.010
34. Bhagwan J, Han JI (2023) Probing the supercapacitive properties of hydrothermal routed MWCNTs@Cd0.98MoO4:Eu3+0.02 nanoparticles. Surf Interfaces 36:102605. https://doi.org/10.1016/J.SURFIN.2022.102605
35. Saratale RG, Hwang K-J, Song J-Y et al (2016) Electrochemical oxidation of phenol for wastewater treatment using Ti/PbO2 electrode. J Environ Eng 142:04015064. https://doi.org/10.1061/(ASCE)EE.1943-7870.0001007
36. Wang J, Jiang Z, Zhang Z et al (2009) Study on inorganic oxidants assisted sonocatalytic degradation of acid red B in presence of nano-sized ZnO powder. Sep Purif Technol 67:38–43. https://doi.org/10.1016/J.SEPPUR.2009.03.005
37. Liu W, Zhou J, Zhou J (2019) Facile fabrication of multi-walled carbon nanotubes (MWCNTs)/α-Bi2O3 nanosheets composite with enhanced photocatalytic activity for doxycycline degradation under visible light irradiation. J Mater Sci 54:3294–3308. https://doi.org/10.1007/s10853-018-3090-x
38. Kermani M, Kakavandi B, Farzadkia M et al (2018) Catalytic ozonation of high concentrations of catechol over TiO2@Fe3O4 magnetic core-shell nanocatalyst: optimization, toxicity and degradation pathway studies. J Clean Prod 192:597–607. https://doi.org/10.1016/J.JCLEPRO.2018.04.274
39. Abdel-Wahab MS, Jilani A, Yahia IS, Al-Ghamdi AA (2016) Enhanced the photocatalytic activity of Ni-doped ZnO thin films: morphological, optical and XPS analysis. Superlattices Microstruct 94:108–118. https://doi.org/10.1016/j.spmi.2016.03.043
40. Saratale RG, Hwang K-J, Song J-Y et al (2015) Electrochemical oxidation of phenol for wastewater treatment using Ti/PbO2

electrode. J Environ Eng 142:04015064. https://doi.org/10.1061/(ASCE)EE.1943-7870.0001007
41. Khataee A, Saadi S, Safarpour M, Joo SW (2015) Sonocatalytic performance of Er-doped ZnO for degradation of a textile dye. Ultrason Sonochem 27:379–388. https://doi.org/10.1016/j.ultsonch.2015.06.010
42. Khataee A, Rad TS, Vahid B, Khorram S (2016) Preparation of zeolite nanorods by corona discharge plasma for degradation of phenazopyridine by heterogeneous sono-Fenton-like process. Ultrason Sonochem 33:37–46. https://doi.org/10.1016/j.ultsonch.2016.04.015
43. Calimli MH, Nas MS, Burhan H et al (2020) Preparation, characterization and adsorption kinetics of methylene blue dye in reduced-graphene oxide supported nanoadsorbents. J Mol Liq 309:113171. https://doi.org/10.1016/j.molliq.2020.113171
44. Manjunath SV, Tripathy BK, Kumar M, Pramod S (2020) Simultaneous degradation of anionic and cationic dyes from multi-dye systems using falling film photoreactor: performance evaluation, kinetic and toxicity analysis. J Environ Chem Eng 8:104486. https://doi.org/10.1016/j.jece.2020.104486
45. Chandhru M, Rani SK, Vasimalai N (2020) Reductive degradation of toxic six dyes in industrial wastewater using diaminobenzoic acid capped silver nanoparticles. J Environ Chem Eng 8:104225. https://doi.org/10.1016/j.jece.2020.104225
46. Chatterjee S, Chatterjee T, Woo SH (2010) A new type of chitosan hydrogel sorbent generated by anionic surfactant gelation. Bioresour Technol 101:3853–3858. https://doi.org/10.1016/j.biortech.2009.12.089
47. Alkan M, Çelikçapa S, Demirbaş Ö, Doğan M (2005) Removal of reactive blue 221 and acid blue 62 anionic dyes from aqueous solutions by sepiolite. Dye Pigment 3:251–259. https://doi.org/10.1016/J.DYEPIG.2004.07.018
48. Mongalo NI, Dikhoba PM, Soyingbe SO, Makhafola TJ (2018) Antifungal, anti-oxidant activity and cytotoxicity of South African medicinal plants against mycotoxigenic fungi. Heliyon. https://doi.org/10.1016/j.heliyon.2018.e00973
49. Zhang X, Ding Y, Tang H et al (2014) Degradation of bisphenol A by hydrogen peroxide activated with CuFeO2 microparticles as a heterogeneous Fenton-like catalyst: efficiency, stability and mechanism. Chem Eng J 236:251–262. https://doi.org/10.1016/J.CEJ.2013.09.051
50. Majhi D, Samal PK, Das K et al (2018) α-NiS/Bi2O3 nanocomposites for enhanced photocatalytic degradation of tramadol. ACS Appl Nano Mater 2:395–407. https://doi.org/10.1021/ACSANM.8B01974
51. Shinde SG, Patil MP, Do KG, Shrivastava VS (2020) Multi-doped ZnO photocatalyst for solar induced degradation of indigo carmine dye and as an antimicrobial agent. J Inorg Organomet Polym Mater 30:1141–1152. https://doi.org/10.1007/s10904-019-01273-2
52. Salih Nas M, Kaya H (2021) Synthesis and sonocatalytic performance of bimetallic AgCu@MWCNT nanocatalyst for the degradation of methylene blue under ultrasonic irradiation. Inorg Nano-Metal Chem 51:614–626. https://doi.org/10.1080/24701556.2020.1799406
53. Sajjadi S, Khataee A, Kamali M (2017) Sonocatalytic degradation of methylene blue by a novel graphene quantum dots anchored CdSe nanocatalyst. Ultrason Sonochem 39:676–685. https://doi.org/10.1016/j.ultsonch.2017.05.030
54. Areerob Y, Cho JY, Jang WK, Oh WC (2018) Enhanced sonocatalytic degradation of organic dyes from aqueous solutions by novel synthesis of mesoporous Fe3O4-graphene/ZnO@SiO2 nanocomposites. Ultrason Sonochem 41:267–278. https://doi.org/10.1016/J.ULTSONCH.2017.09.034
55. Zaman S, Zhang K, Karim A et al (2017) Sonocatalytic degradation of organic pollutant by SnO2/MWCNT nanocomposite. Diam Relat Mater 76:177–183. https://doi.org/10.1016/j.diamond.2017.05.009
56. Zhang K, Zhang FJ, Chen ML, Oh WC (2011) Comparison of catalytic activities for photocatalytic and sonocatalytic degradation of methylene blue in present of anatase TiO2-CNT catalysts. Ultrason Sonochem 18:765–772. https://doi.org/10.1016/j.ultsonch.2010.11.008
57. Nuengmatcha P, Chanthai S, Mahachai R, Oh WC (2016) Sonocatalytic performance of ZnO/graphene/TiO2 nanocomposite for degradation of dye pollutants (methylene blue, texbrite BAC-L, texbrite BBU-L and texbrite NFW-L) under ultrasonic irradiation. Dye Pigment 134:487–497. https://doi.org/10.1016/J.DYEPIG.2016.08.006
58. Darvishi Cheshmeh Soltani R, Jorfi S, Ramezani H, Purfadakari S (2016) Ultrasonically induced ZnO-biosilica nanocomposite for degradation of a textile dye in aqueous phase. Ultrason Sonochem 28:69–78. https://doi.org/10.1016/j.ultsonch.2015.07.002
59. Wu Y, Song L, Zhang S et al (2013) Sonocatalytic performance of AgBr in the degradation of organic dyes in aqueous solution. Catal Commun 37:14–18. https://doi.org/10.1016/j.catcom.2013.03.027
60. Kaya MT, Calimli MH, Nas MS (2023) Degradation of methylene blue with a novel Fe3O4/Mn3O4/CuO nanomaterial under sonocatalytic conditions. Res Chem Intermed. https://doi.org/10.1007/s11164-023-04964-1
61. Bagal MV, Lele BJ, Gogate PR (2013) Removal of 2,4-dinitrophenol using hybrid methods based on ultrasound at an operating capacity of 7 L. Ultrason Sonochem 20:1217–1225. https://doi.org/10.1016/J.ULTSONCH.2013.01.015
62. Lopez-Lopez C, Martín-Pascual J, Martínez-Toledo MV et al (2015) Kinetic modelling of TOC removal by H2O2/UV, photo-Fenton and heterogeneous photocatalysis processes to treat dye-containing wastewater. Int J Environ Sci Technol. https://doi.org/10.1007/s13762-015-0755-8
63. Xu L, Wang J (2012) Fenton-like degradation of 2,4-dichlorophenol using Fe3O4 magnetic nanoparticles. Appl Catal B Environ 123–124:117–126. https://doi.org/10.1016/J.APCATB.2012.04.028
64. Bae S, Kim D, Lee W (2013) Degradation of diclofenac by pyrite catalyzed Fenton oxidation. Appl Catal B Environ 134–135:93–102. https://doi.org/10.1016/j.apcatb.2012.12.031
65. Chiou CH, Wu CY, Juang RS (2008) Influence of operating parameters on photocatalytic degradation of phenol in UV/TiO2 process. Chem Eng J 139:322–329. https://doi.org/10.1016/j.cej.2007.08.002
66. Zhang N, Zhang Y, Pan X et al (2012) Constructing ternary CdS–graphene–TiO2 hybrids on the flatland of graphene oxide with enhanced visible-light photoactivity for selective transformation. J Phys Chem C 116:18023–18031. https://doi.org/10.1021/JP303503C
67. Jia L, Wang D-H, Huang Y-X et al (2011) Highly durable N-doped graphene/CdS nanocomposites with enhanced photocatalytic hydrogen evolution from water under visible light irradiation. J Phys Chem C 115:11466–11473. https://doi.org/10.1021/JP2023617
68. Duan Q, Ji J, Hong X et al (2020) Design of hole-transport-material free CH3NH3PbI3/CsSnI3 all-perovskite heterojunction efficient solar cells by device simulation. Sol Energy 201:555–560. https://doi.org/10.1016/j.solener.2020.03.037
69. Zhang G, Gao Y, Zhang Y, Guo Y (2010) Fe2O3-Pillared rectorite as an efficient and stable Fenton-like heterogeneous catalyst for photodegradation of organic contaminants. Environ Sci Technol 44:6384–6389. https://doi.org/10.1021/ES1011093
70. Huang R, Fang Z, Yan X, Cheng W (2012) Heterogeneous sono-Fenton catalytic degradation of bisphenol A by Fe3O4 magnetic

nanoparticles under neutral condition. Chem Eng J 197:242–249. https://doi.org/10.1016/j.cej.2012.05.035
71. Khataee A, Gholami P, Vahid B (2016) Heterogeneous sono-Fenton-like process using nanostructured pyrite prepared by Ar glow discharge plasma for treatment of a textile dye. Ultrason Sonochem 29:213–225. https://doi.org/10.1016/j.ultsonch.2015.09.012
72. Baldrian P, Merhautová V, Gabriel J et al (2006) Decolorization of synthetic dyes by hydrogen peroxide with heterogeneous catalysis by mixed iron oxides. Appl Catal B Environ 66:258–264. https://doi.org/10.1016/j.apcatb.2006.04.001
73. Hasanvandian F, Shokri A, Moradi M et al (2022) Encapsulation of spinel CuCo2O4 hollow sphere in V2O5-decorated graphitic carbon nitride as high-efficiency double Z-type nanocomposite for levofloxacin photodegradation. J Hazard Mater 423:127090. https://doi.org/10.1016/J.JHAZMAT.2021.127090
74. Fard SG, Haghighi M, Shabani M (2019) Facile one-pot ultrasound-assisted solvothermal fabrication of ball-flowerlike nanostructured (BiOBr)x(Bi7O9I3)1–x solid-solution for high active photodegradation of antibiotic levofloxacin under sun-light. Appl Catal B Environ 248:320–331. https://doi.org/10.1016/J.APCATB.2019.02.021
75. Isari AA, Moradi S, Rezaei SS et al (2021) Peroxymonosulfate catalyzed by core/shell magnetic ZnO photocatalyst towards malathion degradation: enhancing synergy, catalytic performance and mechanism. Sep Purif Technol 275:119163. https://doi.org/10.1016/J.SEPPUR.2021.119163
76. Hayati F, Khodabakhshi MR, Isari AA et al (2020) LED-assisted sonocatalysis of sulfathiazole and pharmaceutical wastewater using N, Fe co-doped TiO2@SWCNT: optimization, performance and reaction mechanism studies. J Water Process Eng 38:101693. https://doi.org/10.1016/J.JWPE.2020.101693